RESEARCH PAPER

Characterization of friction stir-based linear continuous joining of aluminium alloy to structural polymer

Prabilson Khadka[1] · Sean Varglund[1] · Samuel Akinwamide[1] · Pedro Vilaça[1]

Abstract

Dissimilar continuous joining of lightweight metal alloys to structural polymer is a major manufacturing challenge, demanding feasible and reliable solutions. Through-slot extrusion joining (TSEJ) is a friction stir-based processing technique investigated in the manufacturing of continuous linear joints between aluminium alloy AA5754 overlapping structural polymer polyether ether ketone (PEEK). An intermediate rigid and thin titanium extrusion die protects the polymer locally from thermal degradation and promotes the formation of a continuous double hook-like feature of extruded aluminium into the polymer component along the joint path. The structure of the joint provides macro-mechanical interlocking between the joined components. A set of four tools, and other key process parameters, were investigated for process stability, tensile-shear strength, and microstructure. The best TSEJ condition is chosen for microstructural analysis via optical microscopy and scanning electron microscopy. Three distinct failure modes were identified. The best condition provided an average tensile-shear load of 110 kN/m. The tool position with bias toward the flow side of the extrusion slot shows to improve the strength of joints. The microstructural analysis along the interface of AA5754 to PEEK exhibits micro-mechanical interlocking, intercalated layers of these materials and adhesion as joining mechanisms.

Keywords Through-slot extrusion joining · Friction stir-based processing · (IIW Thesaurus:) Dissimilar materials · Metal-polymer joint · Aluminium alloy · AA5754-H111 · Structural polymer · PEEK

1 Introduction

An increasing need for more environmentally friendly and lightweight material technology has established a trend of using high-performance materials, thus increasing the implementation of hybrid metal-polymer structures [1]. The design freedom and high specific strength afforded by structural polymers and polymer composites are complemented by the strength performance and aesthetics of lightweight metals, such as aerospace-grade aluminium alloy. These hybrid polymer-metal joints represent a new category of high-performance parts and assemblies for use in the design of the next generation of technological innovation

✉ Pedro Vilaça
pedro.vilaca@aalto.fi

1   Department of Mechanical Engineering, School of Engineering, Aalto University, Espoo, Finland

[2]. However, several challenges exist for creating these structures of dissimilar materials. One of such challenges is the chemical incompatibility between metals and polymers which prevents strong atomic bonding at their interface [3, 4]. Therefore, polymers and metals are primarily joined using adhesive bonds [5] and mechanical joining [6]. Due to the performance and manufacturing productivity drawbacks of these options, several clinching-based techniques and friction-based spot joining solutions have been recently developed for metal-to-polymer joining [7]. The strength, durability and reliability issues of adhesives are coupled with long processing times and reliability issues related to environmental factors such as heat, temperature, moisture, solvents, and other diluents [8]. Moreover, mechanical fastening introduces disadvantages such as stress concentration, notch sensitivity, and extra weight into a system by increasing total part count alongside increased production costs in the form of assembly time [1]. Mechanical interference alone may be achieved by traditional processes, such as using fasteners [8–11]. Processes such as laser welding [12, 13] and additive manufacturing [14] have been shown

to create adhesive bonds between the metal and polymer components by melting the polymer component with the introduction of heat and allowing re-solidification of the molten polymer at the joining interface.

The application of pressure and heat can create similar adhesive bonds, with examples being friction lap welding [15, 16], and ultrasonic welding [17]. In addition to the adhesive bonding achieved by the melting of the polymer, some processes also introduce bulk material deformation, or clinching, of the metal to achieve varying degrees of mechanical interlocking between sub-components. These are obtained in processes including friction spot joining [18], friction riveting [19], friction stir lap joining [20, 21], and through-hole extrusion welding (THEW) [22] utilizing non-consumable tools to heat and stir the metal and polymer materials.

A comprehensive review of different techniques used to join hybrid metal-to-polymer structures and the current technological gaps is established by Barakat et al. [23]. The increasing need of lightweight hybrid structures, and difficulties of fusion welding processes in joining dissimilar materials, which are inherent to the significant role posed by the different physical properties of materials, pushes solid state-based techniques to evolve as solution for joining hybrid structures. Rudrapati [24] emphasizes how the selection of process parameters plays an important role in the stability and strength of the joints manufactured using friction-stir welding (FSW). Renangi et al. [25] provide an overview on the applications of FSW to produce hybrid joints between thermoplastic polymer and metal in sectors, such as automobile and aerospace, due to its high strength to weight ratio. Renangi et al. [25] also address the role of the hybrid structures in future innovations and need further research on the relation between intermixing, flow pattern, microstructure features, and mechanical properties to support the transition of hybrid structure manufactured by FSW, into industrial applications. The issue of overflowing polymer, which often results in the unconsolidated top surface of the processed domain, is relevant in most emerging metal-to-polymer friction stir-based techniques [26–28].

Currently, no industrially established joining technique provides continuous, durable, stable, and structurally strong joints for metal-to-polymer hybrid structures. Through-slot extrusion joining (TSEJ) [29] is a friction stir-based solution aiming to cover this perceived need. This metal-to-polymer joining technique is an evolution of THEW technique and uses a non-consumable tool [30], similar to the ones used in friction stir-based techniques [31], to extrude a part of the viscoplasticized processed metal into the polymer. The resultant features of the interface between the dissimilar materials deliver strong fastener-free joints along a linear continuous free path. This work presents the investigation of TSEJ application to join aluminium alloy AA5754-H111

to unreinforced polyether ether ketone (PEEK) structural polymer. The research plan aims to investigate the technological influence of key process parameters on the TSEJ joint strength. For this purpose, four tensile-shear specimens are extracted from each joint, to provide statistical relevance to the results from mechanical testing. The research plan explores the influence of four tools, with different probe geometries, and travelling at three different positions relative to the axis of the slot of the extrusion die. The joining mechanisms of the strongest joint are assessed via microstructural analysis. The shape and depth of the hook-like feature and heat flow effect on the polymer degradation are also assessed.

2 Through-slot extrusion joining (TSEJ)

Previous art exists for the joining of metals to polymers. However, they mostly cover non-continuous joining, e.g. via spot joining. Hence, there is a perceived need for linear continuous manufacturing solutions delivering reliable and high-strength joints. TSEJ is designed to be such a solution. TSEJ is a new manufacturing technique used to produce continuous joints between a metallic component and a polymer-based component in an overlap-joint configuration. TSEJ is a variant of friction stir-based processing applied to a metal lap joint to polymer that was developed at Aalto University by Vilaça et al. [FI 20227037] [29]. The TSEJ process is an evolution of the through hole extrusion welding (THEW) [WO2019002693 A1] [22]. The TSEJ method uses a thin rigid extrusion die sub-component providing a continuous open-through slot. The rigid extrusion die is as-thin-as-possible and made of a material with thermomechanical properties providing negligible deformation during the joining process. The thin rigid extrusion die sub-component is positioned in-between the overlapping metallic and polymeric component. The portion of metallic component being processed by the tool softens as a result of the heat energy released during its bulk plastic deformation. This portion of viscoplasticized metal is then forced through the continuous slot of the rigid extrusion die into the polymer-based component, as depicted in Fig. 1.

The rigid rotating tool is plunged into the metallic component and travels along the same path of the continuous slot. During the processing phase of the TSEJ, the tool shoulder keeps the top surface of the metallic component closed, and the tool probe produces a viscoplastic deformation of the metallic component. The metallic component is forced to flow through the slot of the thin rigid extrusion die into the polymer. The local interaction between the viscoplasticized metal and the polymer results in the formation of a joint. During processing, molten polymer fills a void in the metallic component, forming a non-uniform mass of

Fig. 1 Schematic illustration of the new friction stir-based continuous joining process of aluminium alloy to structural polymer: through-slot extrusion joining (TSEJ). **a** Components and parameters of the process in a continuous linear joint. **b** Typical cross-section with the formation of the mechanical interlocking based on a hook-like feature. **c** The TSEJ applied in a continuous non-linear joint
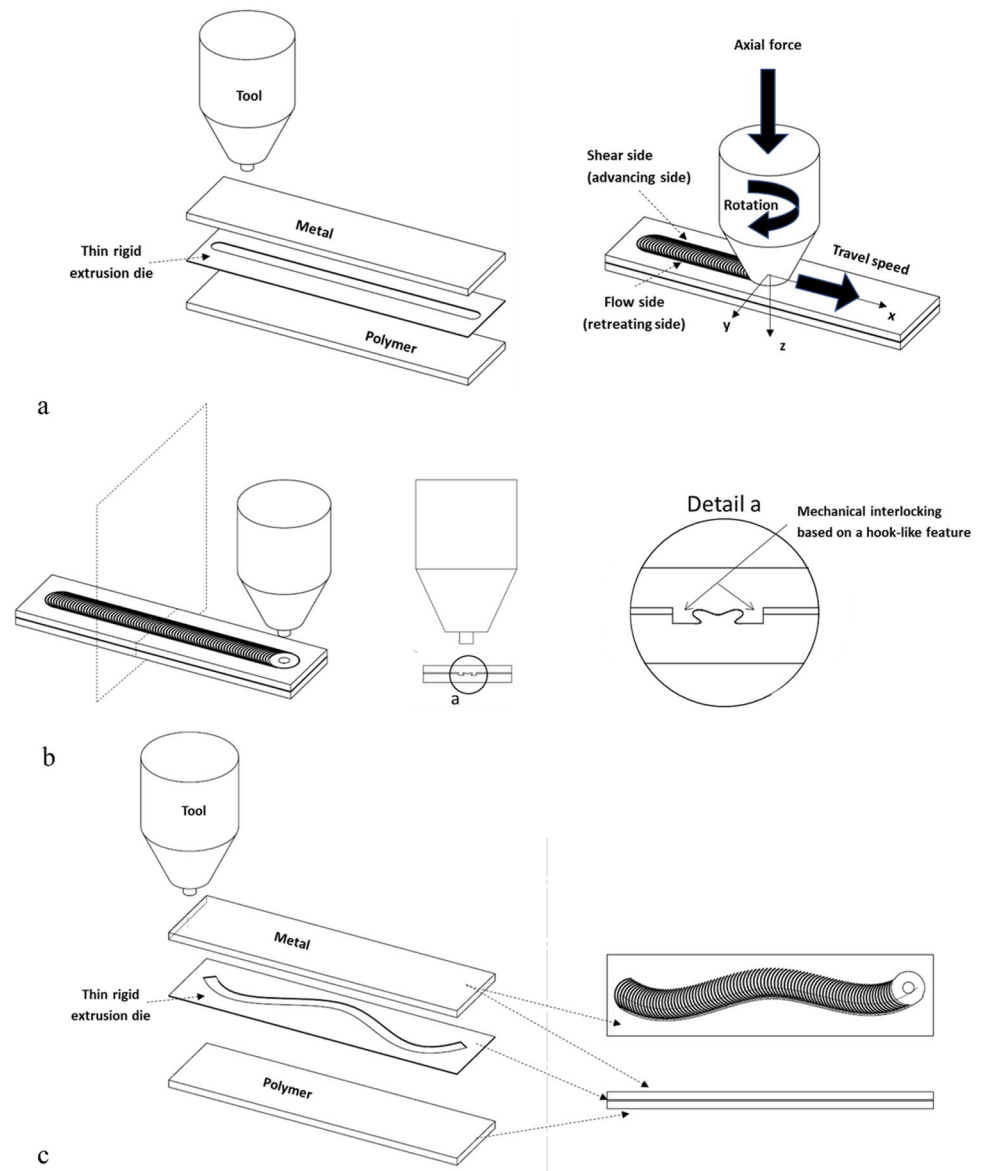
polymer between two hook-like protrusions of the metallic component, which resemble the shape of a crab's claw. The double hook or crab claws shape (details in Fig. 1), which is filled with the polymer-based component, forms a strong mechanical interference known as clinching. The joining mechanisms of TSEJ result from this strong macro- and micro-mechanical interference, with the additional contribution of the physical and chemical adhesive and diffusion phenomena at the contacting interface between the metallic component and the polymer-based component. If the metal being joint to the polymer-based component is an aluminium alloy, and the thin rigid extrusion die is made of titanium, with about ten times lower thermal conductivity than the aluminium, then the thin rigid extrusion die also protects the polymer-based component from any large-scale thermal degradation. The thin rigid extrusion die also prevents large

range softening of the polymer, avoiding relaxation of the clamping forces, and keeping stable the forging load applied by the tool on the components. Another benefit from the thin rigid extrusion die is that while the small slot enables the aluminium to be extruded into the polymer-based component, it prevents a large-scale upflow of polymer into the metallic processed zone. Therefore, the shoulder-to-metal interface is kept free of the mobilized polymer.

3 Materials and methods

3.1 Materials

The technical details of each base material AA5754-H111 (5-mm thick plate), PEEK (5-mm thick plate), and titanium

grade 1 (0.6-mm thick sheet metal) used for producing the TSEJ specimens are presented in Table 1. The AA5754 is a solid-solution strengthened aluminium alloy, with magnesium as the main alloying element, which gives it a good combination of enhanced mechanical properties and corrosion resistance [32]. The H111 designation indicates a small amount of strain hardening is applied to the material.

As the energy dissipation inherent to the bulk deformation of AA5754 results in local temperatures that far exceed the melting temperature of the polymer, the PEEK in close vicinity with the extruded part of the AA5457 undergoes melting with partial volatilization. Thus, the consolidation of the joint depends on the thermoplastic ability of the PEEK to be reprocessed through the melting point. The low thermal conductivity and high operational thermal resistance are beneficial to preserve the bulk of the polymer component from excessive temperature and deformation, respectively. Furthermore, the non-toxicity of PEEK results in safe work conditions around the material during processing when combined with proper ventilation of the polymer vapours. This material is addressed in depth in the literature [33, 34]. Some relevant properties of natural non-reinforced PEEK used for the work are presented in Table 1.

Titanium exhibits a relatively low thermal conductivity and high melting point compared to most of the engineering metals. It is for these properties, alongside the relatively high strength of titanium versus the AA5754 and PEEK, at the TSEJ processing temperature domain, that the material was selected as thin rigid extrusion die for this TSEJ processing. The titanium strips used in TSEJ act as a heat insulator and impediment to material flow in the areas directly adjacent to the joining zone. These physical properties preserve the polymer from large-scale thermal degradation and deformation. As it will be addressed later in the analysis of microstructural results § 4.4, only the polymer in direct contact with the stirred aluminium will undergo degradation. Simultaneously, the stiff titanium dies aid in shaping the flow of aluminium as it penetrates the polymer component. Other relevant properties of titanium grade 1 are shown in Table 1.

3.2 Experimental setup and TSEJ constant parameters

TSEJ test setup utilized a lap joint configuration as depicted in Fig. 2. The aluminium alloy and polymer are assembled with the 0.6-mm titanium extrusion die strips inserted into milled channels in the interfacial face of the PEEK. A 3-mm diameter blind pre-hole at the plunge position is drilled into the aluminium plate, penetrating slightly into the PEEK component. The joining parameters which were constant during the experiments are presented in Table 2. Four different probe shapes and three different positions of the tool centre relative to the centre of the slot formed by thin titanium strips were tested. One joint for each process permutation was made, for a total of 12 joints of 130-mm length, as represented in Fig. 3. Each joint was produced with a clean shoulder and probe.

3.3 TSEJ variable parameters and sample identifier

The quality of the TSEJ joints will be evaluated from the result of the tensile-shear strength test in addition to visual inspection, macrographs, and the micrographs obtained from optical and scanning electron microscopy (SEM) analyses of the aluminium-PEEK interfaces. The specific process variations used in this study are as follows:

1. Changes to tool probe shape < *ToolID* > in Table 4. The effect of tool geometry (via the shape of the probe) on joint quality is coupled with the effect of penetration depth into the polymer by the probe.
2. Changes to the position of the tool within the TSEJ extrusion die slot < *SlotCondition* > in Table 3. The position of the centre of the tool relative to centre of the thin rigid extrusion die slot centre (Fig. 2) is also evaluated, as it affects the pattern of extruded AA5754 into the PEEK component.

The tensile-shear test samples and OM imaging are conducted on specimens extracted from the same joints. The
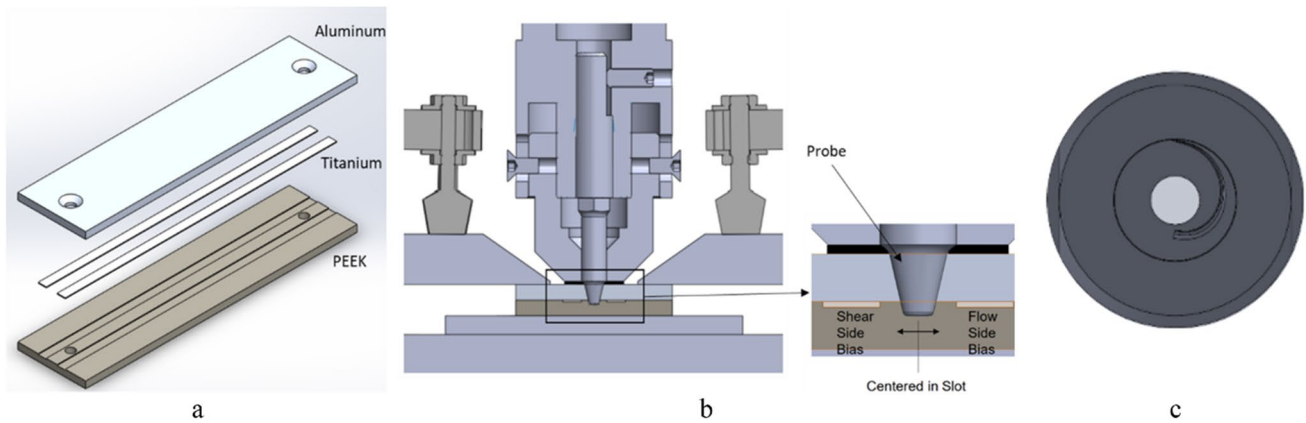
Table 1 Relevant material properties of AA5754-H111, PEEK, and Titanium Gr 1 [35–37]

Properties	AA5754-H111	PEEK	Ti Gr 1
Density [g/cm^3]	2.68	1.31	4.51
Thermal conductivity [W/(m.K)]	132	0.25	17
Coefficient of thermal expansion [μm/(m.K)]	23.7	-	8.4
Solidus/liquidus [°C]	595/645	-	-
Heat capacity [kJ/(Kg.K)]	-	1.34	-
Glass transition temperature [°C]	-	143	-
Melting Temperature [°C]	-	343	1670
A50 Elongation [% min]	18	-	-
Elongation at break [%]	-	20	-
Tensile strength [MPa]	190–240	-	-
Yield stress [MPa]	-	87–110	Min 170

Fig. 2 Representation of the key components and system for implementation of the TSEJ. **a** The three components necessary for the TSEJ processing are shown graphically. The top component is AA5754-H111 aluminium alloy plate, followed by two thin strips of titanium grade 1, and the PEEK polymer plate. The dimensions of the aluminium and PEEK are $200 \times 60 \times 5$ [mm], and the titanium strips shown are $200 \times 10 \times 0.6$ [mm]. **b** A CAD rendering of a cross-section of the process setup, including clamps, the tools mounted on a modular tool holder post, and the workpieces. On the side is an enlarged view of the position of the probe relative to the thin titanium strips: centred in the slot. **c** Tool's shoulder

Table 2 TSEJ process parameters kept constant in test trials

TSEJ process parameters	Value
Rotational speed, $\Omega_{spindle}$ [rpm]	600 CW
Travel speed, v_{weld} [mm/min]	140
Shoulder: diameter [mm]	16.0
Shoulder: nominal penetration into workpiece [mm]	0
Tool tilt angle [°]	0
Tool plunge speed [mm/s]	0.1
Dwell time [s]	3.5
Acceleration time/length [s]/[mm]	7.7/9.0
Deceleration time/length [s]/[mm]	3.0/3.5
Process control (Z axis)	Position

tensile-shear samples are produced from each joint in the sequence shown in images in Fig. 3. Between the second and third samples, a 10-mm section of the joint is reserved for OM analysis. The nomenclature of these samples is as follows:

- Table 4 Tool ID (Table 4) and extrusion slot position ID (Table 3) extension to build the final unique sample ID in the form:

$< ToolID > < SlotPosition > < .SequenceNumber >$. An example of a unique sample ID is T1+1.3 which would refer to the third tensile-shear specimen from the start of the joint made with the T1 probe (Tref), with flow side biased (1 mm toward the flow side in the extrusion slot).

- Samples for microscopy analysis are only one per trial condition and thus, they are labeled with the tool ID and slot extension in the form: $< ToolID > < SlotPosition >$. Sample T2-1 would represent the joint made with the T2 probe (Tref − 1 mm), with shear side biased (1 mm toward the shear side in the extrusion slot).

3.4 Tensile-shear test samples

The tensile-shear and microscopy samples are extracted from the joints as illustrated in Fig. 3. The tensile-shear specimen geometry is alternated in orientation between even and odd samples. This alternating geometry produced the following pulling load conditions:

- Flow side by the edge (BTE) of the PEEK = Flow side BTE
- Shear side by the edge (BTE) of the PEEK = Shear side BTE

This method is used to investigate the different responses of the joint to pulling load direction with respect to the substructures of the TSEJ joint. The test samples produced in positions 1 and 3 are of the form *Flow side* by the edge (*BTE*) of the PEEK, while samples in positions 2 and 4 are of the counterpart geometry: *Shear side* by the edge (*BTE*) of the PEEK.

The dimensions of the tensile-shear specimen follow the standard tensile-shear specimen geometric reference guide for spot welds based on ISO 14273:2016 [38]. Dimensions of 60 mm × 24 mm (width × length, respectively) were applied to each numbered sample (Fig. 3). The overlap between components in the joint is 20 mm,

Fig. 3 Sample's extraction plan from test specimen for microscopy analysis (M) and 4 samples for tensile-shear strength testing, at different positions along the joint and with different pulling load conditions, namely flow/shear side by the edge (BTE) of the PEEK
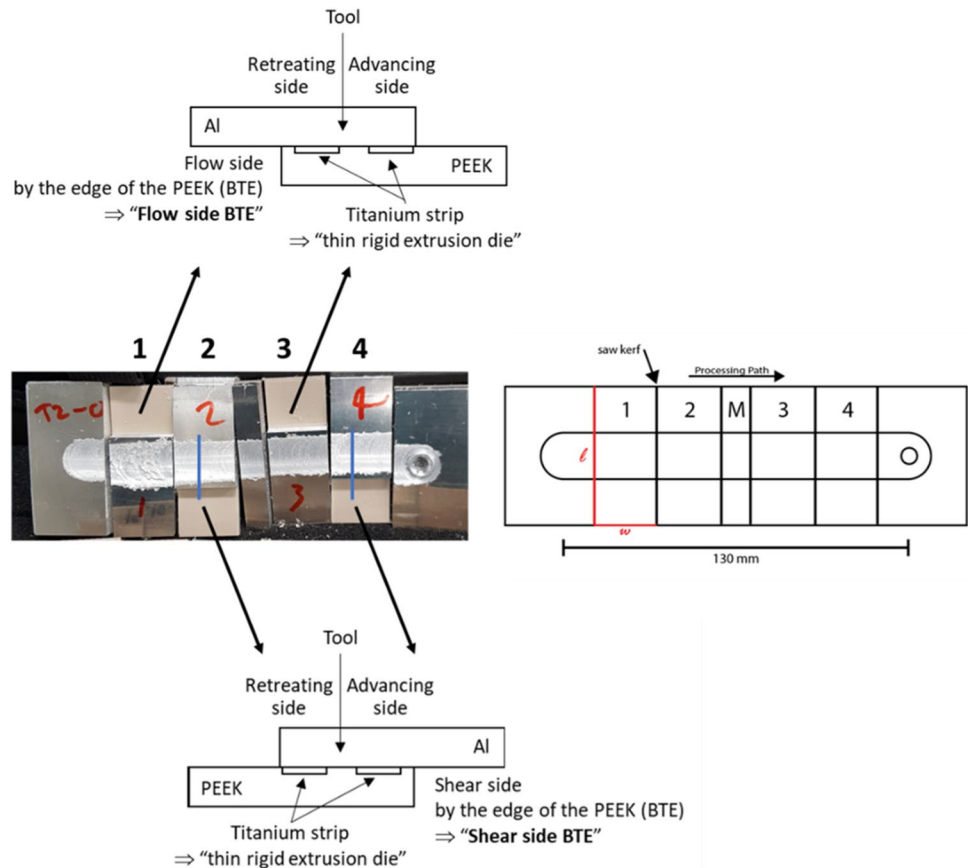

Table 3 The position of the TSEJ processing tool relative to the thin rigid extrusion die slot and their tool ID extension used for organizing the results

Slot condition	1 mm shift toward shear side (or advancing side) *Shear side biased*	*Centred in slot*	1 mm shift toward flow side (or retreating side) *Flow side biased*
Tool ID modifier	− 1	0	+ 1

and the free length between clamps is 22 mm. Furthermore, sample M with a length of 10 mm shown in Fig. 3 was used for microstructural analysis.
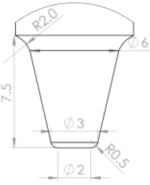
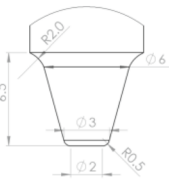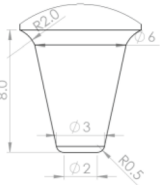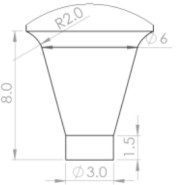### 3.5 Tensile-shear strength analysis

The tensile-shear strength tests are performed with the Zwick Roell and MTS testing systems. To make meaningful comparisons between the different samples within each set of joints and across the different test sample geometries, a length-normalized load value is used to compare the maximum load characteristics. The processing of the values obtained from the four different specimens extracted from

each test trial will be presented in terms of the maximum tensile-shear strength and deformation at fracture for the average ($\mu \equiv$ representing 50% of the population) and for average minus one standard deviation ($\mu - \sigma \equiv$ representing 84% of the population). According to Fig. 3, and within each one of the 12 specimens, produced with different set of parameters, the population is 4 testing samples. To aid in parsing the data points in graphic plots, the box-and-whisker plot is used for tensile-shear load data.

3.6 Microscopy analysis

The samples for optical microscopy and scanning electron microscopy (SEM) analysis are extracted from the centre of the 12 joints of interest and mounted in Struers EpoFix (cold) resin. These mounted samples are polished using the Struers Tegramin-20. The samples and machine are cleaned with water in between polishing steps to prevent cross-contamination of abrasives and slurry material across grit size changes. The first step in grinding is with an abrasive surface of about 220 grit lubricated with water until surface disparities caused by the machining of the samples are removed. This was followed by polishing using 9, 3, and 1 µm diamond suspension until a mirror-like surface was achieved. Finally, the samples were rinsed in ethanol and

Table 4 Tool probe geometries used in the evaluation of TSEJ joints

Tool ID	T1	T2	T3	T4
CAD drawing				
Probe length (T1 = 7.5 mm)	**T1 = Tref**	**T2 = Tref−1mm**	**T3 = Tref+0.5mm**	**T4 = Tref−1mm+cyl**
Polymer penetration [mm]	1.5	0.5	2.0	2.0

dried with warm air. Special attention is taken to prevent water from the crevices and holes of the samples around the titanium extrusion dies and joint formation from drying onto the surface of the polished samples. For proper microstructural examination, the inspected surface of the samples was dipped in Keller's reagent for 20 s, rinsed in warm water, and dried. Optical micrographs were captured using the Zeiss Stemi 508 stereo-microscope and Zeiss Vert.A1. Macrostructures of the joint were observed under bright-field lighting, dark-field lighting, and polarized light. SEM examination was conducted using a Zeiss field electron VP Merlin Compact scanning electron microscope. SEM analysis was only focused on the best-performing condition, sample T1 + 1. The surface of the sample was coated with a 20-mm thick carbon layer to prevent charging and improve the conductivity of the non-conductive polymer component during examination.

4 Results and discussion

4.1 Surface characterization

The images in Fig. 4 represent the visual examination of the top surface of the joint (shoulder processed surface) in the as-processed condition. This characterization provides insights on notable qualities and possible defects of TSEJ joints visually identifiable from the top surface of the joints. Recall the nomenclature for the unique sample IDs as put forth in § 3.3.

Sample T1-0 is the reference condition, or go-to average, regarding surface quality observed in TSEJ joints of metal-to-polymer at the time of publication. The evidence of the tool action, mostly via de shoulder (Fig. 2c), over the top surface of the metallic material is considered normal state-of-the-art, for processing with zero tilt angle. There should be continuity of the surface, without any significant

expulsion of metal into flash, near the edges. The ability of the tool to close the ceiling of the joint, as depicted in Fig. 4, is an evidence that the TSEJ is stable for the tested probe geometries. The primary factor determining the stability of the ceiling is likely a combination of shoulder design and balance of heat input through control of process parameters. This observation comes in part as a result of the experience gained while developing the shoulder features and set of process parameters for this study.

At the plunge position (i.e. at the start of the processing path), occasional imperfections in the joint surface are visible. At this plunge zone, if the heat of the process builds up excessively and there is a large probe plunge depth into the polymer-based component, the polymer undergoes vaporization. Vaporous and molten polymer flowing upwards toward the shoulder may prevent consolidation of the processed surface at the start of the joint. In general, at the start of the joint path, the process passes through a transition, evolving from the hotter axisymmetric processing of the plunging phase into the processing of the colder material until it reaches the steady-state condition, after about two shoulder diameters. The samples from the trial with the smaller probe length, i.e. the T1 reference sample family and T2 sample family, have the most consistent and even surface finish. When the probe is increased in size and length, as in the T3 sample family, the flash production is increased, and the joint takes longer to reach stability. This fact is also more evident for the trials with + 1 mm shift toward flow side (or retreating side), the "flow side biased" trials. The occasional discontinuity at the plunge domain of the processed path can be addressed by further optimizations of the process parameters such as pre-hole dimensions, probe length optimization, tool plunge speed, dwell time, and acceleration up to travel speed.

The roughness of the surface in the centre of the processed zone corresponds to the frequency, or weld pitch, of the shoulder action over the surface of the

Fig. 4 Collection of the images from the top surface of all the 12 different conditions test trials. Every image is matched to the corresponding unique sample identifier as described in § 3.3
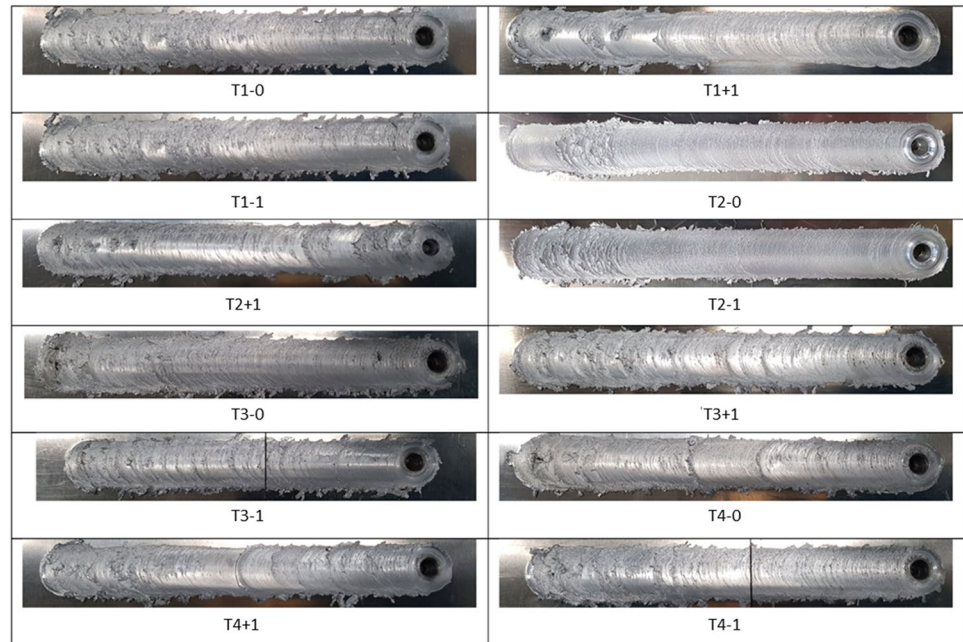
aluminium, as the rotating tool travels along the joint: Weld pitch = Travel speed [mm/min]/Rotational speed [rpm] = 140/600 = 0.23 mm. The flash is a ribbon-like continuous material, formed in layers for each weld pitch of the tool shoulder. The ridges at the centre vary in height from experiment to experiment and even across the length of individual joints. This is not due to any inconsistence during the "position control" of the joints, as established in Table 2, but due to the small "run-to-run variance" phenomenon of cumulative adhesion of aluminium to the tool shoulder followed by the sudden release of a critical amount of accumulated material. The small "run-to-run variance" exists in all friction stir-based welding procedures and is more relevant when processing with null tilt angle (Table 2). The Z position is kept constant, with a value equal to the probe length (Table 4), so that the shoulder nominal penetration into workpiece is kept at 0 mm in all trials (Table 2). Due to the small "run-to-run variance", the axial Z position is kept constant at the cost of some variance of the axial Z force and spindle torque ($T_{spindle}$), as depicted in Fig. 5. The small "run-to-run variance" is more evident in trials with longest probes (Table 4), such as the T4-based trial samples: T4-0, T4 + 1, and T4-1.

Based on Fig. 5, the heat input (HI) value calculated during the TSEJ is in average of about 485 J/mm, corresponding to a mechanical power (P_{mech}), delivered by the tool into the workpieces is in average of about 1.13 kW, during the quasi-stable joining period. The mechanical power (P_{mech}) is calculated via the following: P_{mech} [W] = $T_{spindle}$ [N.m] × $\Omega_{spindle}$ [rpm] × 2π /60. The heat input (HI) is determined via the following: HI [J/mm] = P_{mech} [W] × 60/v_{weld} [mm/min].

4.2 Tensile-shear strength analysis

4.2.1 Failure modes

The metal-to-polymer joints produced for tensile-shear strength analysis express three distinct modes of failure, as geometrically depicted and characterized in Fig. 6. These failure modes are governed by the following conditions:

- The depth, shape, and surface roughness of the hook-like feature, affect the level of strength of the metal-to-polymer mechanical interlocking, enable to reach the Failure Mode 3 (the strongest one, with combined resistance to shear and cross-tension stress);
- The level of heat transferred into the polymer component, affects the level of degradation of the polymer, and reduces the wetting of the metallic surface by the liquid polymer, therefore, reducing the adhesive bonding efficiency governs mostly the Failure Mode 1 (typically strongest under largely dominant pure shear stress);
- The level of consolidation of the joining at the top surface of the metallic component in the joint governs mostly the Failure Mode 2 (typically the weakest one, also with less elongation at maximum load).

Along one joint path, different types of failure mode mechanisms can be observed. This behaviour is because the thermomechanical boundary conditions are never perfectly uniform along the joints and the sensitivity of joining metal-to-polymer is sensitive to this phenomenon. The thermal boundary conditions are not uniform, e.g. due to the shape of the components which affects differently the heat flow
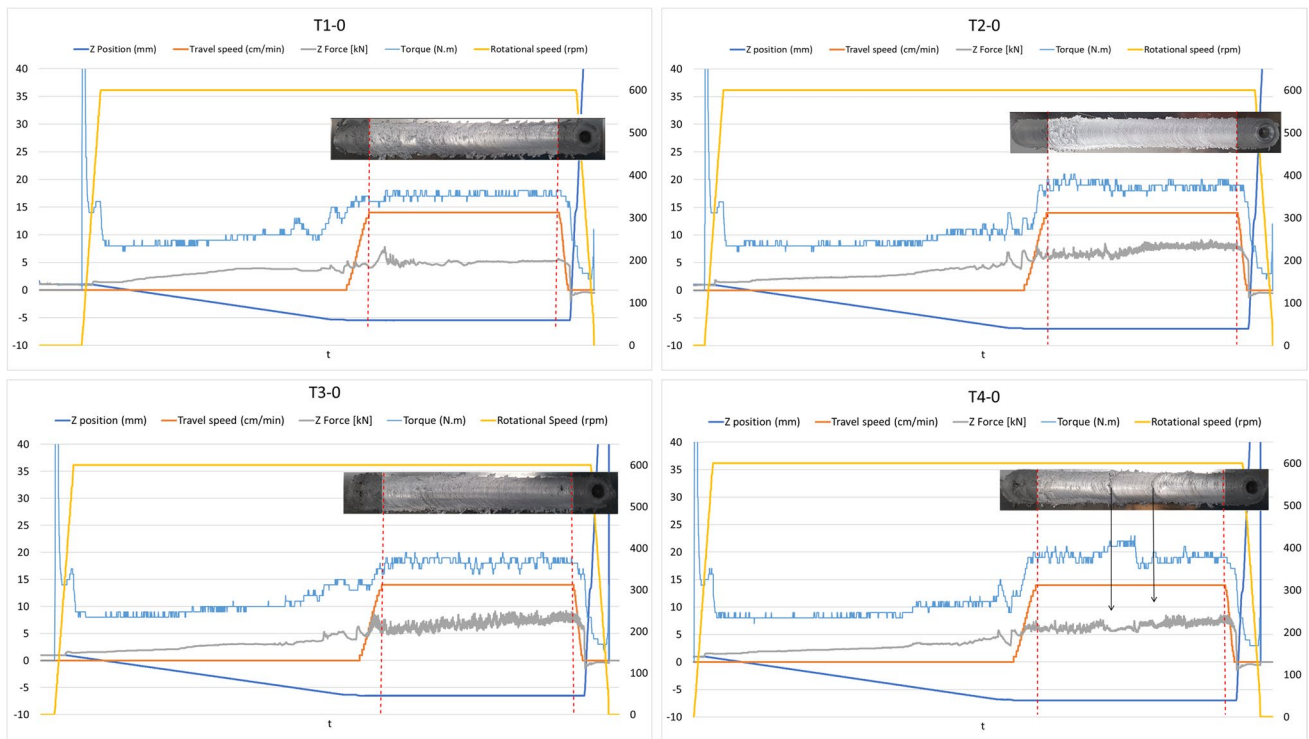
Fig. 5 Data from online monitoring (over time, at a rate of 10 Hz) of main TSEJ process parameters during testing for all four probe geometries, with tool aligned with centre of the slot (T1-0, T2-0, T3-0, and T4-0): axial Z force [kN], Z position (Z [mm]), rotational speed ($\Omega_{spindle}$ [rpm]), spindle torque ($T_{spindle}$ [N.m]), and travel speed (v_{weld} [cm/min])
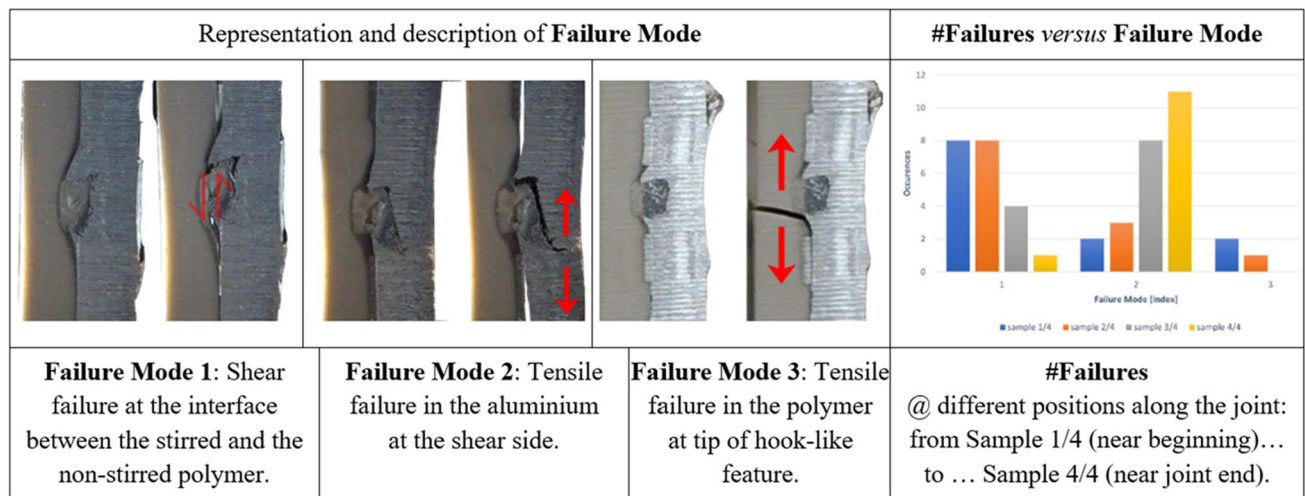

Fig. 6 Different failure modes found in TSEJ joints when tested for tensile-shear strength, with red arrows to represent the relevant areas and type of dominant stress in the failure mechanism

during the heat source travel along the path of the joint, and mechanical boundary conditions are not uniform, e.g. due to non-perfectly rigid and uniform mechanical clamping. Figure 6 includes the relationship between failure modes and the specimen index. For the lower strength joints, as it progresses from the plunge to the exit point, the frequency of failure mode occurrences shifts from most dominant Failure Mode 1, presenting shear failure at the interface between the stirred and the non-stirred polymer domain and aligned with the tip of the relatively closed and not very deep hook-like

feature, to primarily Failure Mode 2, that of failure in the aluminium at the shear side, due to insufficient consolidation of the ceiling of the metallic stirred zone (SZ). Furthermore, Failure Mode 3 is only present in the first two sample positions. A possible explanation for this phenomenon is that the lower temperature of the process near the beginning may reduce the volume of molten PEEK, consequently less molten polymer and polymer vapours will mobilize upward and affect the consolidation of the shear side of the aluminium. When process time increases and there is more heat accumulation in the system, some excessive polymer vaporization may reduce the full consolidation of the aluminium at the shear side of the joint ceiling, thus reducing local strength and promoting Failure Mode 2.

The length-normalized tensile-shear strength of all 12 of the T-series joint conditions [kN/m] and elongation at maximum load [mm] is presented in Tables 5 and 6, respectively. The statistical values for each trial condition are obtained from four test trials' data as established in § 3.3 and depicted in Fig. 3. The T1 + 1 condition (highlighted in bold) exhibits the overall best strength and ductility average (μ), and this phenomenon is further emphasized with the calculation of the average minus one standard deviation (μ − σ).

Illustrated in Fig. 7a is the trend of a reduction in mean tensile-shear strength from the start of a TSEJ joint toward the end. This data encapsulates the entire series of tests and thus has many underlying factors affecting the results.

Nevertheless, the effects should be evenly represented in each of the positions along the joint. The mean tensile-shear strength of each sample in the sequence appears to level off at an asymptotic value above 60 kN/m. Figure 7b emphasizes the influence of the tool probe position within the slot of the thin rigid extrusion die. As previously emphasized in Table 5, the flow side biased position (+ 1) leaves space for the extrusion-driven formation of the hook-like feature at the shear side. This position thus delivers the best overall performance of length-normalized tensile-shear strength. The shear side biased (− 1) position should be avoided.

The relationship between maximum sustained tensile-shear load and elongation is made in Fig. 8 with a scatter plot and regression. The relationship which emerges is an increasingly positive relationship between elongation at max load and max sustained load. This interpretation is complemented by analysis of the failure modes. The plot sets depicted in Fig. 9 demonstrate the differences in maximum sustained load when categorized by Failure Mode 1 to 3. All samples, which failed in Failure Mode 3, sustained high loads with flow BTE (by the edge) pulling load condition, presenting the best results. Failure in the ceiling of the stirred aluminium at the shear side, or Failure Mode 2, breaks with higher mean sustained load in the shear BTE (by the edge) pulling load condition. As would be expected for a pure shear failure mode, for Failure Mode 1, there is no difference in pulling load condition.

Table 5 Length-normalized average tensile-shear strength of all 12 joint conditions

μ − σ [kN/m]	Length-normalized average tensile-shear strength of the 12 test trial conditions		
Tool reference and slot condition	Flow biased (+ 1)	Centred (+ − 0)	Shear biased (− 1)
T1	**(109.9 − 9.7) = 100.2**	(76.1 − 42.0) = 34.1	(47.1 − 23.1) = 24.0
T2	(106.8 − 37.1) = 69.7	(85.6 − 17.6) = 68.0	(65.4 − 7.3) = 58.1
T3	(75.3 − 38.6) = 36.7	(71.8 − 44.3) = 27.5	(48.5 − 13.6) = 34.9
T4	(65.9 − 3.7) = 62.2	(78.1 − 26.2) = 51.9	(61.3 − 11.3) = 50.0

Each condition has four data points obtained from the tensile-shear strength test done in samples with nomenclature as established in § 3.3 and extracted as depicted in Fig. 3

Table 6 Average elongation at maximum load of all 12 joint conditions

μ − σ [mm]	Average elongation at max load of the 12 test trial conditions		
Tool reference and slot condition	Flow biased (+ 1)	Centred (0)	Shear biased (− 1)
T1	**(1.83 − 0.24) = 1.59**	(1.52 − 0.64) = 0.88	(1.40 − 0.20) = 1.20
T2	(1.88 − 0.50) = 1.38	(1.50 − 0.21) = 1.29	(1.19 − 0.27) = 0.92
T3	(1.54 − 0.77) = 0.77	(1.46 − 0.80) = 0.66	(1.21 − 0.61) = 0.60
T4	(1.35 − 0.13) = 1.22	(1.50 − 0.52) = 0.98	(1.31 − 0.40) = 0.91

Each condition has four data points obtained from the tensile-shear strength test done in samples with nomenclature as established in § 3.3 and extracted as depicted in Fig. 3
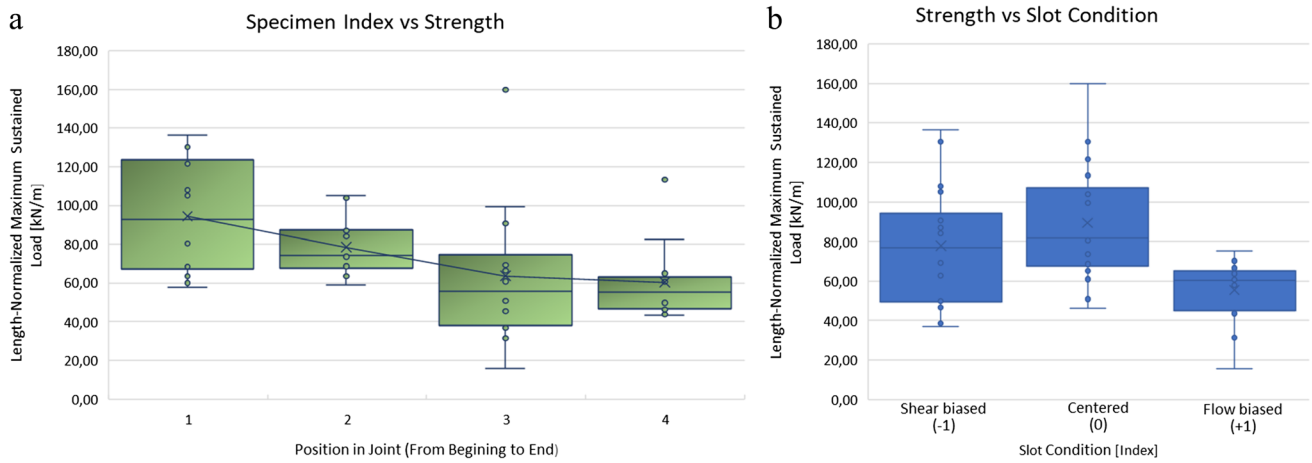
Fig. 7 The Length normalized maximum tensile-shear strength of all 12 joints conditions versus. **a** Sequence of sample position within the specimen, where sample 1 is taken near the beginning of the joint, and sample 4 is taken from near the end). **b** position of the tool probe within the extrusion slot

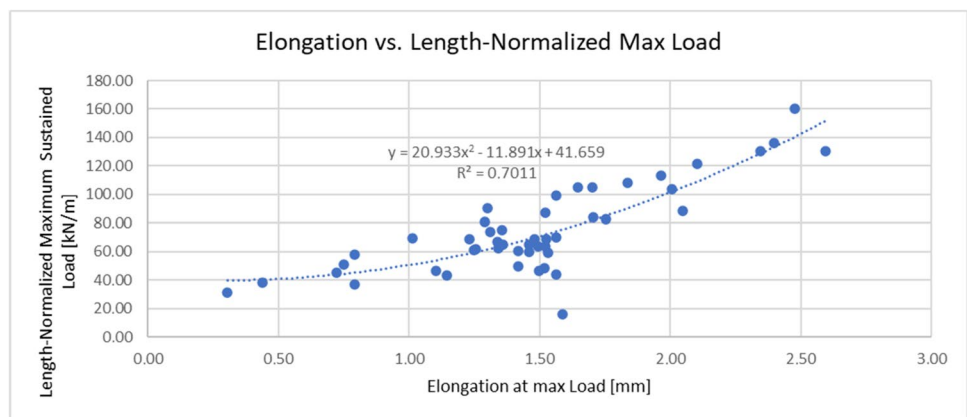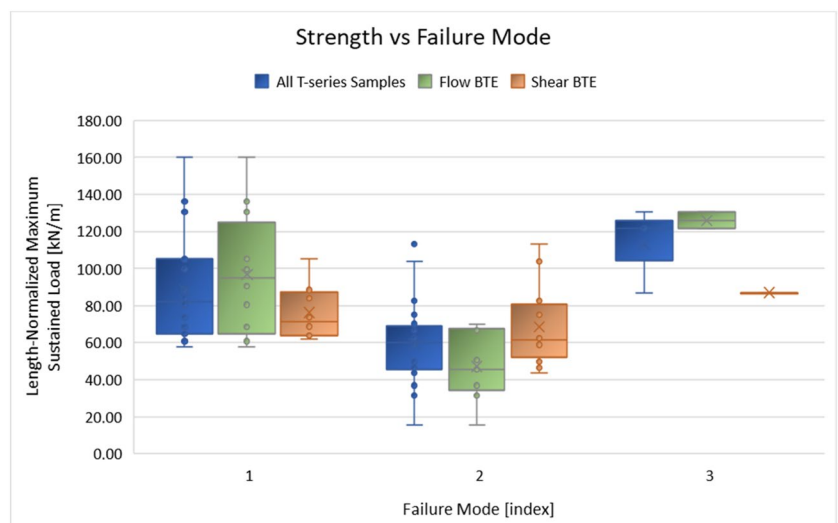**Fig. 8** Length normalized maximum tensile-shear strength plotted versus the elongation at maximum load

Fig. 9 Length normalized maximum tensile-shear strength tests of all 12 joints, displayed by primary Failure Mode 1 to 3, and split between the "flow/shear BTE (by the edge) of the PEEK" pulling load condition of the test samples

4.3 Maximum load contours

The tensile-shear strength test data is further analyzed to focus on the effect of tool geometry and position of the tool in the slot of the rigid and thin extrusion die. Four contour plots are prepared, one for each position along the weld from the beginning to the end, as the pulling load condition alternates between subsequent samples. The charts in Fig. 10 reveal a trend of increased tensile-shear strength toward flow-biased slot condition. In particular, Fig. 10a, for the early portion of the joint (1/4 position samples), reveals a significant reduction of the tensile-shear strength (113 kN/m) going into the shear-biased slot condition. Concerning the influence of the tooling, the shortest tool probe profiles, namely T1 = Tref and T2 ≡

Tref − 1 mm, delivered the best tensile-shear strength performance (from 105 to 160 kN/m) for the mid-portion of the joint (2/4 and 3/4 position samples). The tool T1 = Tref reached the best tensile-shear strength (113 kN/m) for the test samples at the end portion of the joint (4/4 positions). The tool with probe T4 ≡ Tref − 1 mm + cyl consistently revealed the lower performance under tensile-shear strength testing.

The comparison of the length normalized maximum tensile-shear strength against position along joint for all 4 tested tool geometries in the 3 different slot conditions is collected and presented in Fig. 11. The shortest tool probe profiles (T1 = Tref and T2 ≡ Tref − 1 mm) delivered not only the best overall conditions but also the more uniform along the joint. In particular, the T2 ≡ Tref − 1 mm presents the
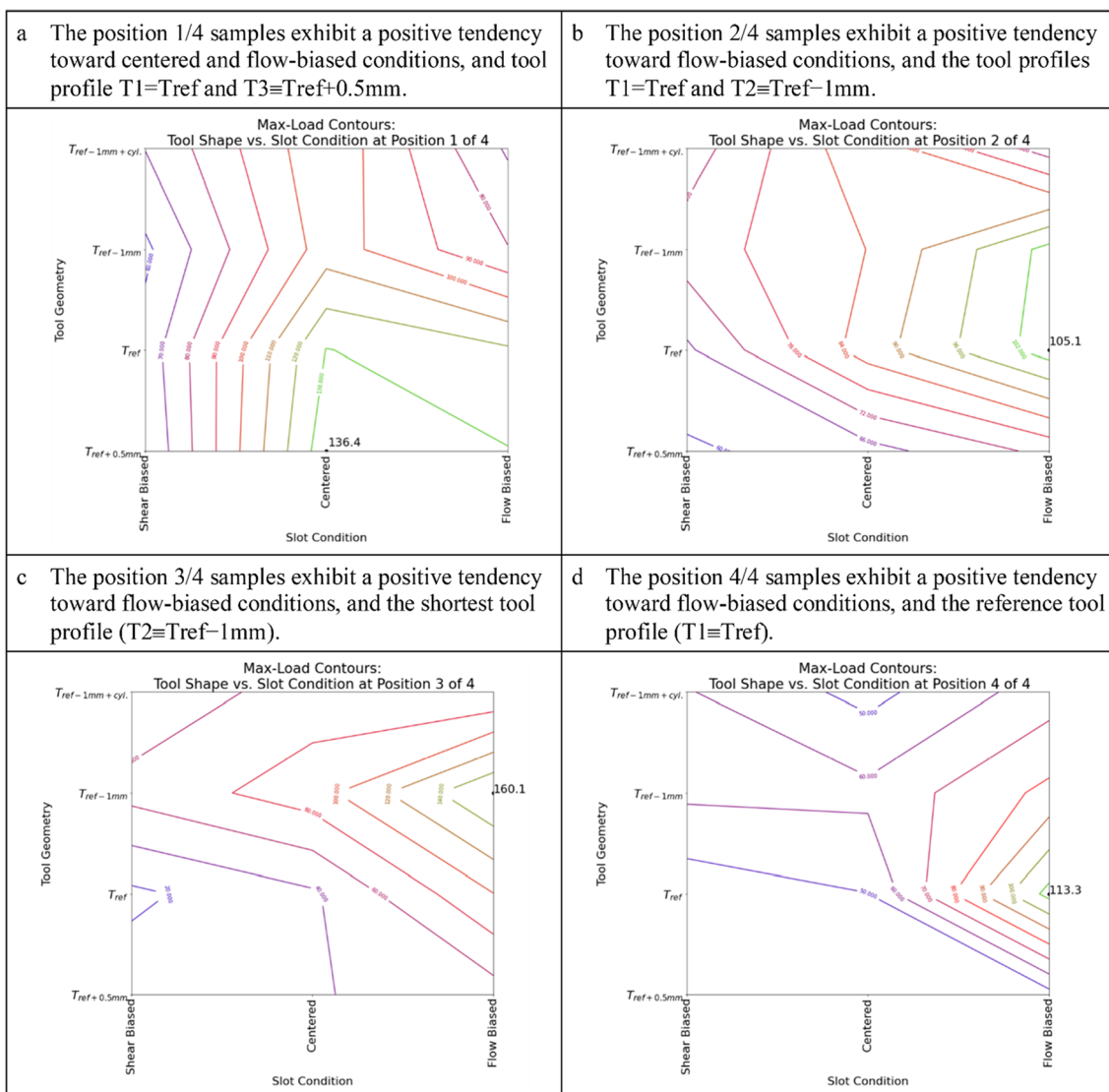

Fig. 10 Length-normalized maximum tensile-shear strength contours plotted as a function of tool geometry and slot condition. The *y*-axis uses nomenclature from Table 4, namely T1 ≡ Tref, T2 ≡ Tref − 1 mm, T3 ≡ Tref + 0.5 mm, and T4 ≡ Tref − 1 mm + cyl

best overall tensile-shear strength performance with 160 kN/m. This value is not a characteristic value of the TSEJ parameters but is due to an extraordinary alignment of the loading and joint Failure Mode 2 in pure shear. The typical tensile-shear strength performance of T2 is overall below the T1, for the flow-biased relative position of the probe in the extrusion slot, which corresponds to the best condition for this position for all tested tool probe geometries. Again, it is confirmed that the tool with probe $T4 \equiv Tref-1\,mm+cyl$ was revealed to consistently deliver the lower performance all along the joint for any relative position of the probe in the extrusion slot. In overall analysis, the $T1+1$ has the highest tensile-shear strength (just below 120 kN/m), which is quasi-uniform all along the joint, even under different pulling load condition of the test samples.

4.4 Summary on the tensile-shear strength properties and failure modes

- The absolute maximum tensile-shear strength obtained from testing all the samples was 160 kN/m. The best joint

condition $(T1+1)$ exhibited an average tensile-shear strength of 110 kN/m.

- Tensile-shear strength increased with increased offset (up to $+1$ mm) of the tool probe towards the flow side within the slot of the rigid thin extrusion die.
- Shorter probes favour colder steady-state processing conditions, but the claw opening is small, preventing the easy flow of the polymer into the hook-like feature domain, resulting in a low level of mechanical interlocking and thus relying almost exclusively on adhesive bonding under pure shear, at the joining interface: Failure Mode 1.
- The intermediate long probes produced a good balance between the claw opening and the limited heat transference into the polymer, resulting in joint samples which failed by tension in the polymer: Failure Mode 3. This condition and associated failure mode are expected to provide also the best resistance to cross-tension loading, in addition to the good level of tensile-shear strength. This is pending on confirmation by future work.
- The design limit for the probe length is set to minimize large heat generation and joint conditions which lead to
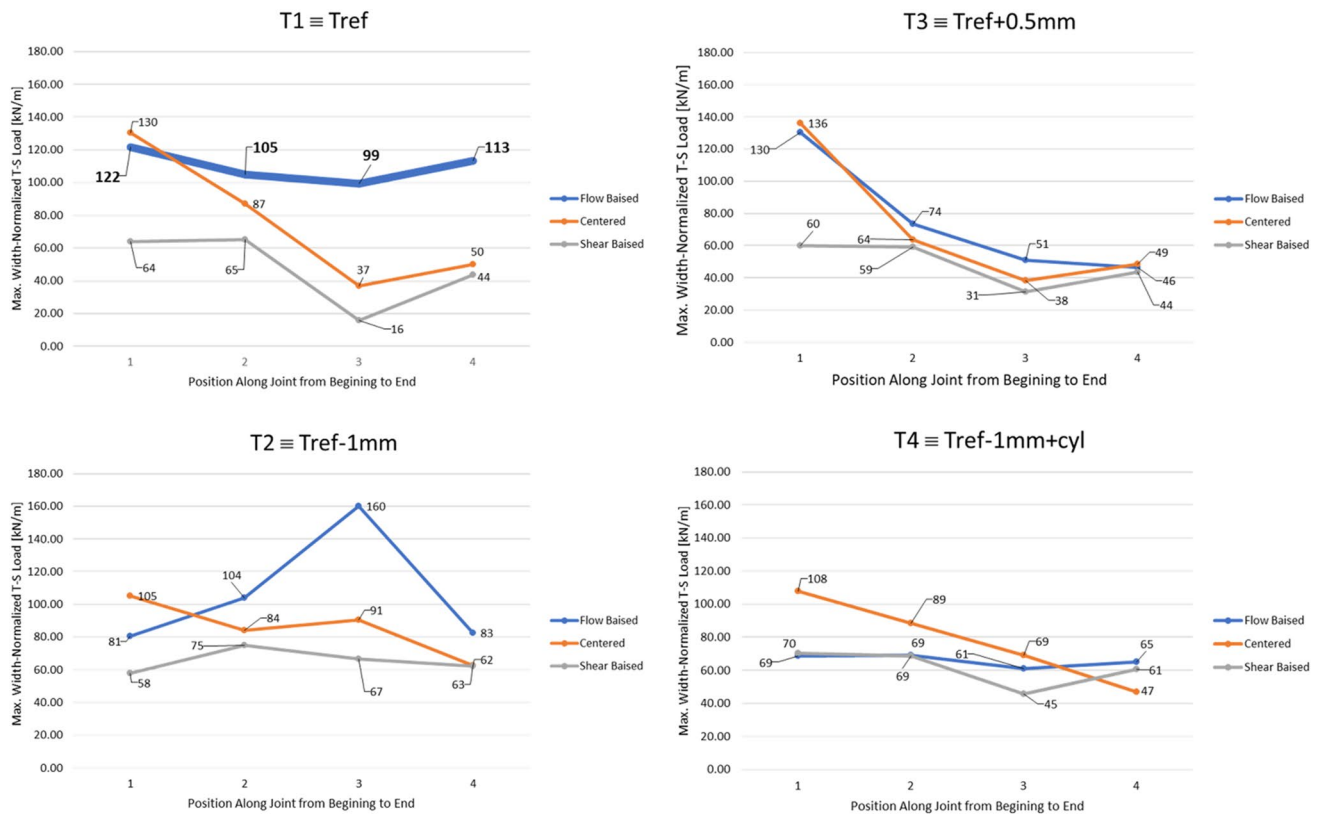

Fig. 11 Comparison of the length-normalized maximum tensile-shear strength against position along joint for all 4 tested tool geometries in the 3 different positions of the tools within the slot. The 4 tested tool probe geometries and respective nomenclature follows

Table 4: Tool probe geometries used in the evaluation of TSEJ joints, namely $T1 \equiv Tref$, $T2 \equiv Tref-1\,mm$, $T3 \equiv Tref+0.5\,mm$, and $T4 \equiv Tref-1\,mm+cyl$. Emphasis on the stable and higher tensile-shear strength performance corresponding to $T1+1$ specimen condition

tensile failure in the aluminium at the shear side (Failure Mode 2). This failure mode is mostly promoted by excessive vaporization and degradation of polymer component.

- The excessive probe length and inherent excessive plunging into the polymer component at the start of the joint also affect the capacity to close the top surface of the joint at the plunge domain. Otherwise, the TSEJ enables to deliver fully sound top surface of the joints, i.e. stable, closed and with negligible flash formation.
- In opposition to the quality of the top surface finishing, there was a slight decrease in tensile-shear strength as the test sample was extracted from areas further away from the start of the joint. This will be of relevance in establishing the characteristic strength in the design of TSEJ joints.

4.5 Macro- and micro-structural analysis

The microstructure of the AA5754/PEEK joining interface was investigated with optical microscopy and SEM. The results encompass images from both macroscopic and microscopic analysis. The macroscopic analysis aims to identify distinct geometrical characteristics of the hook-like feature, and macro-level imperfections, such as particle alignment at the shear side of the aluminium stirred zone and flow, formation of bubbles, and degradation of the polymer within the new open domain of the hook-like feature. The microstructure analysis will focus on the metal/polymer interface of the best-tested condition. The analysis of this interface will provide an insight into the joining mechanism addressed in § 4.2 and tensile-shear mechanical strength evaluated in 4.3.

A collection of cross-sectional macrographs with all 12 tested joints is organized in Fig. 12. Each row corresponds to a tool probe geometry, with nomenclature as established in § 3.3. For each row, the arrangement of images from left to right follows a progression from shear-bias to slot-centred into flow-biased joint formation. The analysis of the cross-sections along the first column, corresponding to the TSEJ joints created with a shear-biased condition (− 1 mm tool offset towards the shear-side of the extrusion slot), exhibits larger voids, mostly located at the flow side of the processed domain. These void zones at the ceiling of the hook-like feature domain indicate incomplete flow of the polymer, as it solidified before completely filling the space created during the formation of this domain. This can be attributed to somewhat lower heat transfer into the PEEK material, resulting from a decreased degree of hot metal extrusion (from the shear side leg of the hook-like feature) into the polymer. In contrast, samples made with flow-biased condition (+ 1 mm offset towards the flow-side of the extrusion slot) exhibit quasi-full filled channels. The extrusion of the aluminium hooks features exhibits increased dimensions and

depth as the joining process transitions from the shear-side to the flow-side of the extrusion, emphasizing the influence of tool offset on the metal and polymer flow. When tool T2 is used, the characteristic open-channel claw structure of the TSEJ technique undergoes a significant transformation into a nearly planar hook structure, with the quasi-closed hook structure allowing only intermittent filling of polymer melt in the hook-like feature domain. This effect is most notable in the centred (− 0) and flow-biased conditions (+ 1). The results of T3 and T4 tools provide complementary phenomena to those obtained with T2. The probes share a similar total length, except T4 has a bossed cylindrical tip. This results in the widely open-channel profiles obtained. The observed cross-sectional geometries are influenced by the design of the probe, not only in total length but also in overall shape. Specifically, the steeper angle at the probe tip, the higher the extrusion force applied downward into the polymer. Some large pores are evident in the polymer component of several TSEJ conditions, but from the analysis of one cross-section only, it is not possible to conclude about the amount and size along the full joint length. In future research approaches, namely targeting fine-tuning of best TSEJ performing conditions, radiographic-based non-destructive testing should be implemented before cutting the samples for destructive-based testing.

From the results of the tensile-shear strength tests presented in § 4.3, the condition T1 + 1 stands out as the only sample which exhibits both the highest strength and ductility levels of all our test conditions. This cross-section presents small-size bubbles in the polymer, which fills a quite symmetric crab shape of the hook-like feature. The condition T1 + 1 is investigated in detail, with additional macrographs, obtained from OM analysis, with focus on Keller's etched aluminium material (Fig. 13) and focus on the polymer material (Fig. 14), using OM with darkfield imaging. The microstructure analysis via SEM of the condition T1 + 1 will focus on the interface of AA5754/PEEK, as depicted in Figs. 16 and 17. The selected locations with most-interest along the joining interface are identified in Fig. 15.

Figure 13 presents a fully consolidated ceiling of the aluminium processed zone. There is a long alignment of particles, uprising from the AA5754/PEEK interface towards the surface and delimiting the shear side of the aluminium stirred zone. The results from mechanical testing show that the well-consolidated part of the aluminium plate thickness is enough to avoid Failure Mode 2, as established in Fig. 6. The extruded hook-like features developed at both sides are quasi-symmetric in depth into the polymer and with well-defined shapes providing a large macro mechanical interlocking.

Figure 14 represents the optical macrograph of the best-performance TSEJ condition T1 + 1. It is possible to evaluate the macro-features of the polymer component at the vicinity

Fig. 12 Optical macrograph of polished cross-sections extracted from the mid-portion of the joint as depicted in sample extraction plan of Fig. 3. The TSEJ samples are identified according to nomenclature in § 3.3. Note that PEEK in the vicinity of the thermomechanical heat-affected zone can turn dark shade of brown. In all photos, the shear side (or advancing side) is on the left, and the flow side (or retreating side) is on the right side of the image
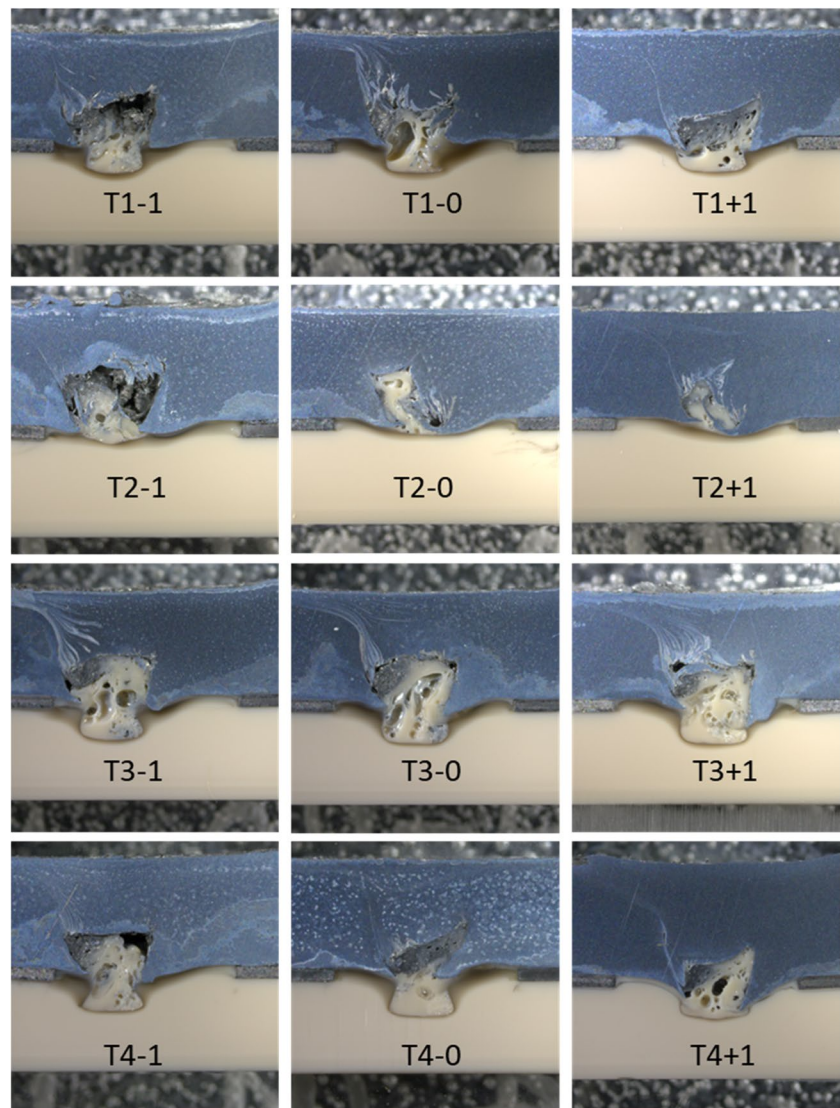

Fig. 13 Optical macrograph of cross-section, extracted from selected best performance TSEJ condition T1 + 1, focused on aluminium component, using polarized and bright-field light, and emphasizing the hook-like feature of extruded aluminium into the polymer component
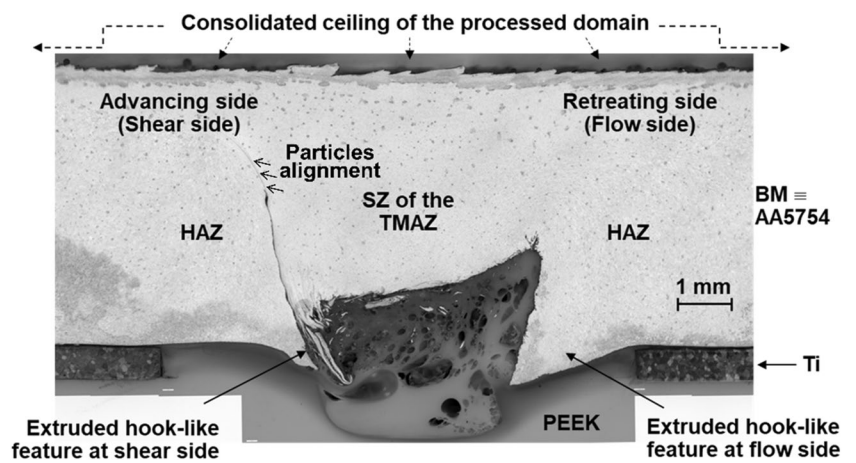
Fig. 14 Optical macrograph of cross-section, extracted from selected best performance TSEJ condition T1 + 1, focused on the PEEK, using darkfield light, and showing a quasi-continuous wetting and adhesion by the PEEK over the surface of AA5754. The detailed view emphasizes the stirred polymer zone including porosity and a few free-aluminium fragments
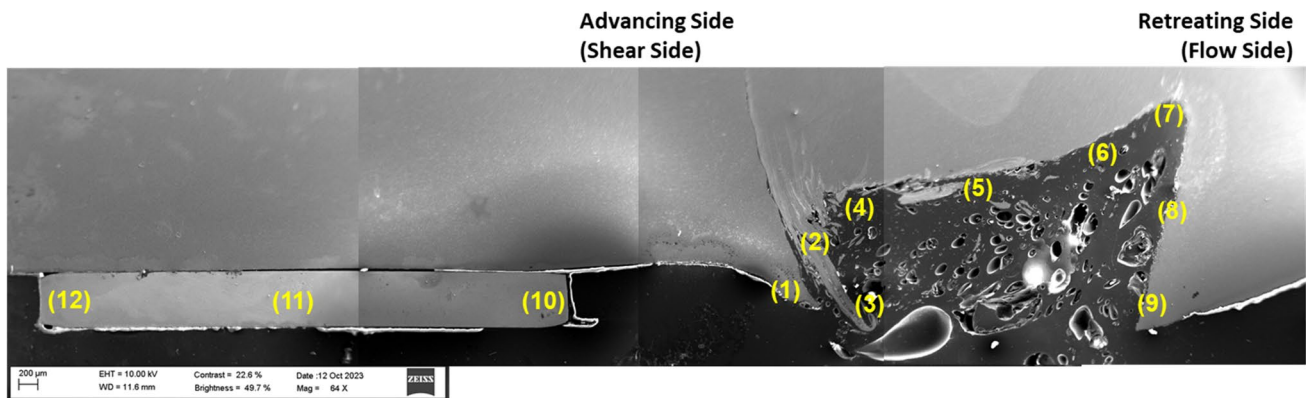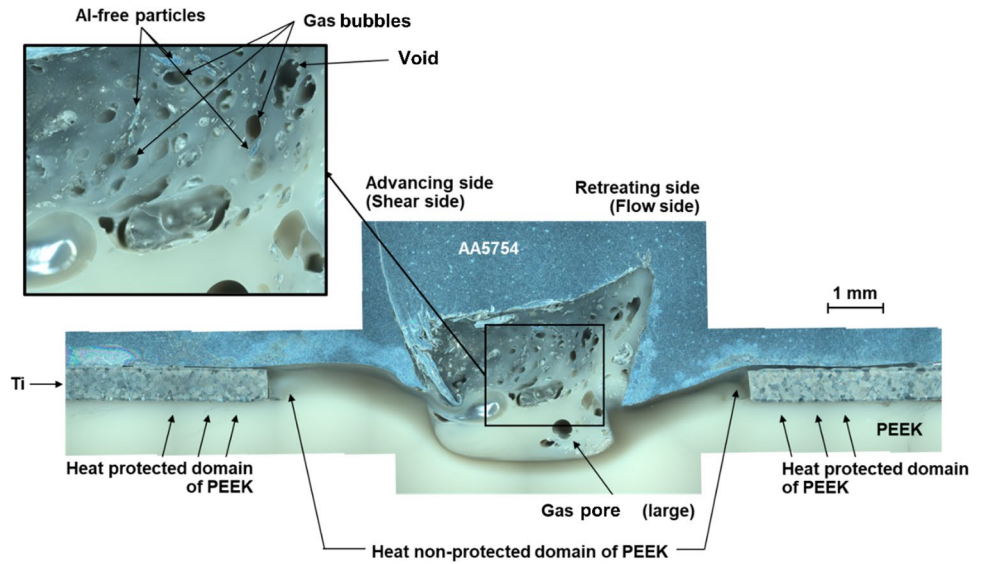

Fig. 15 SEM-based macrograph of cross-section, extracted from selected best performance TSEJ condition T1 + 1, focused on the domain of formation of the hook-like features (areas of interest 1 to 9), and interfaces between the AA5754 and PEEK with the Ti strip forming the rigid extrusion die, at the shear side (areas of interest 10 to 12)

of the interface with the aluminium processed zone and titanium strips. The action by the tip of the probe left a clear mark of the polymer stirred zone. Also, one major result is to confirm that as postulated in the concept of the TSEJ process, the titanium strips, with their low thermal conductivity, indeed protect the polymer from extensive heat affectation. Only the PEEK directly processed by the tool probe or in direct contact with the processed aluminium material undergoes visible evolution into a "dark shade". As emphasized in Fig. 14, some Al-free particles of various sizes and shapes are suspended in a matrix of PEEK. These Al-free particles may eventually contribute as reinforcement particles for the PEEK in this domain. Although with the presence of bubbles and voids, within the domain left open by the formation of the aluminium hook-like features, at this level of magnification, it is evident that most of the aluminium surface is in contact with the polymer. However, occasional gas pockets

or voids can be observed along the metal's surface. Further contact between the AA5754 and the PEEK is observed outside the hook-like feature structure domain between the metal and polymer. This adds evidence to the claimed mechanical interlocking and adhesive bonding contributing simultaneously as primary joining mechanisms of TSEJ joint. These joining mechanisms are also claimed by other authors, such as Klaus et al. [39] and Amancio et al. [40]. This fact will be confirmed later from the SEM analysis.

In general, the gas pockets are located within the PEEK and away from direct contact with the surface. According to Klaus et al. [13], the formation of bubbles is a widely known phenomenon in thermal joining of thermoplastics to metals, with water- and degradation-based gas pockets being the driving mechanisms for this phenomenon. Also, according to Courvoisier et al. [41], the water concentration and diffusion of aromatic linear polymers, such as PEEK, are presumably
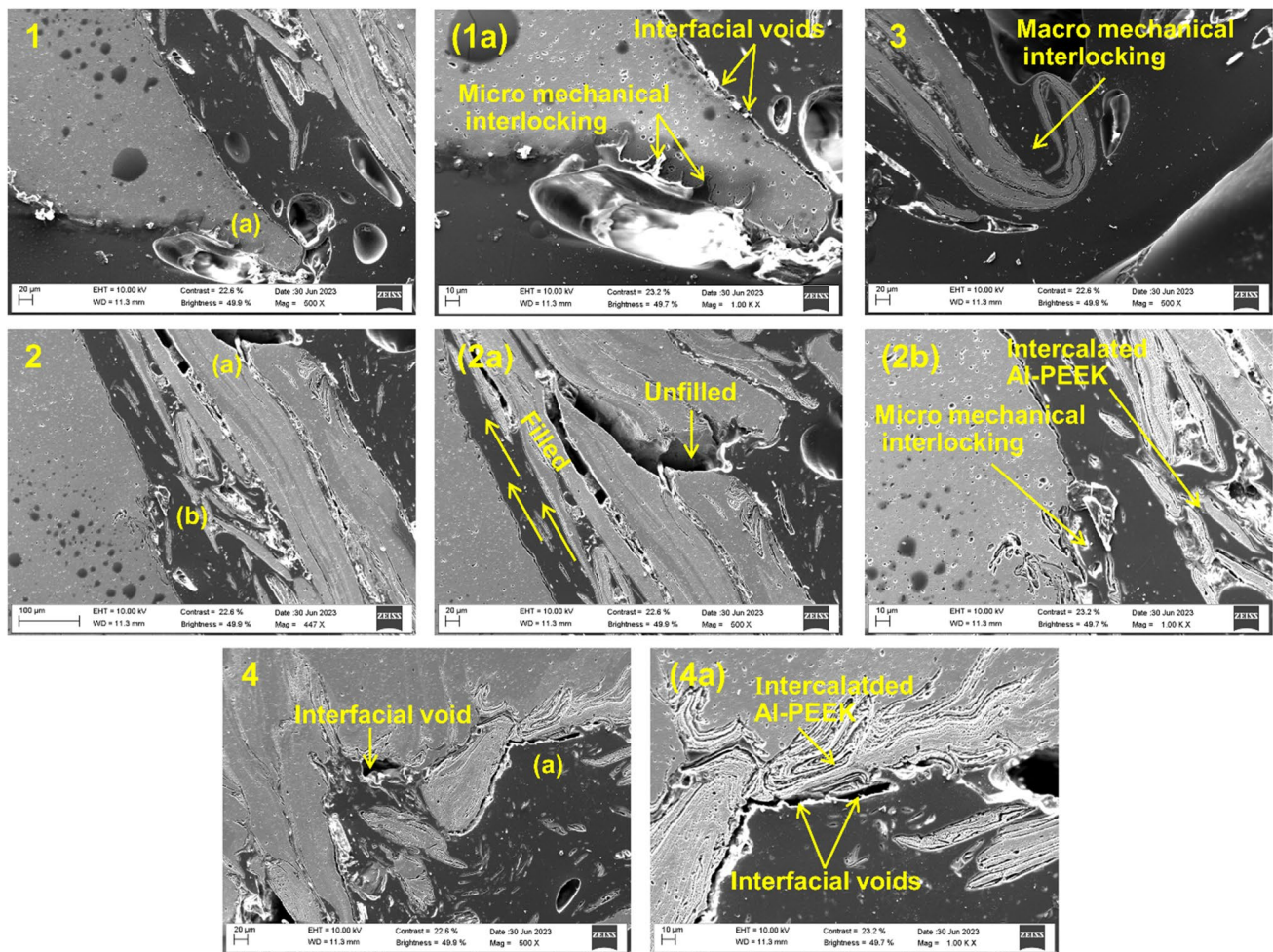
Fig. 16 SEM-based micrographs from points of interest at the interface metal/polymer as identified in Fig. 15 with focus on the shear side (or advancing side)

due to their polar groups establishing molecular interactions with water. Besides the bubbles that are typically gas pockets with smooth surface and quasi-spherical shape, the formation of voids, which are typically gas pockets with irregular surface, is mostly due to shrinkage effects during the cooling process, with or without the contribution from the gases in the origin of the bubbles' formation. The eventual degradation of the polymer is due to high process temperatures transported from the tool probe and the stirred aluminium. Typically, the peak processing temperatures are below the melting temperature of the aluminium alloy being processed but well above the melting of the polymer (Table 1). The assessment of these temperatures is outside the scope of present research methods, but they have been evaluated in previous research work by the authors, namely Vilaca et al. [42, 43].

Figure 15 identifies the sequence and location of the 9 points of interest, along the AA5754/PEEK joining interface, selected for SEM analysis. Figure 15 also includes the zones of interest 10 to 12, addressing the interfaces between

the multimaterial system of overlapping AA5754 with Ti rigid extrusion die, and embedded Ti rigid extrusion die within the PEEK. Because both shear and flow sides present similar phenomena at this multimaterial interface system AA5754/Ti rigid extrusion die/PEEK, the analysis will focus on the shear side (or advancing side).

Figure 16 (details 1a and 3) depicts the composition of micro-mechanical interlocking providing support to the macro-mechanical interlock hook-like feature from the shear side. Among the joining mechanism at the shear side, a large amount of intercalated metal-polymer lamellae structures can be found, as emphasized in Fig. 16 (details 2b and 4a). The polymer presents good overall wettability towards the AA5754, with the viscosity enabling almost full coverage of the metal surface, even though 20-mm narrow open channel (see Fig. 16, detail 2a), but the same figure also depicts one blocked volume that remains unfilled. No bubbles are found at the interface AA5754/PEEK, but few polymer voids can be found at the interface as depicted in Fig. 16 (details 4 and 4a).
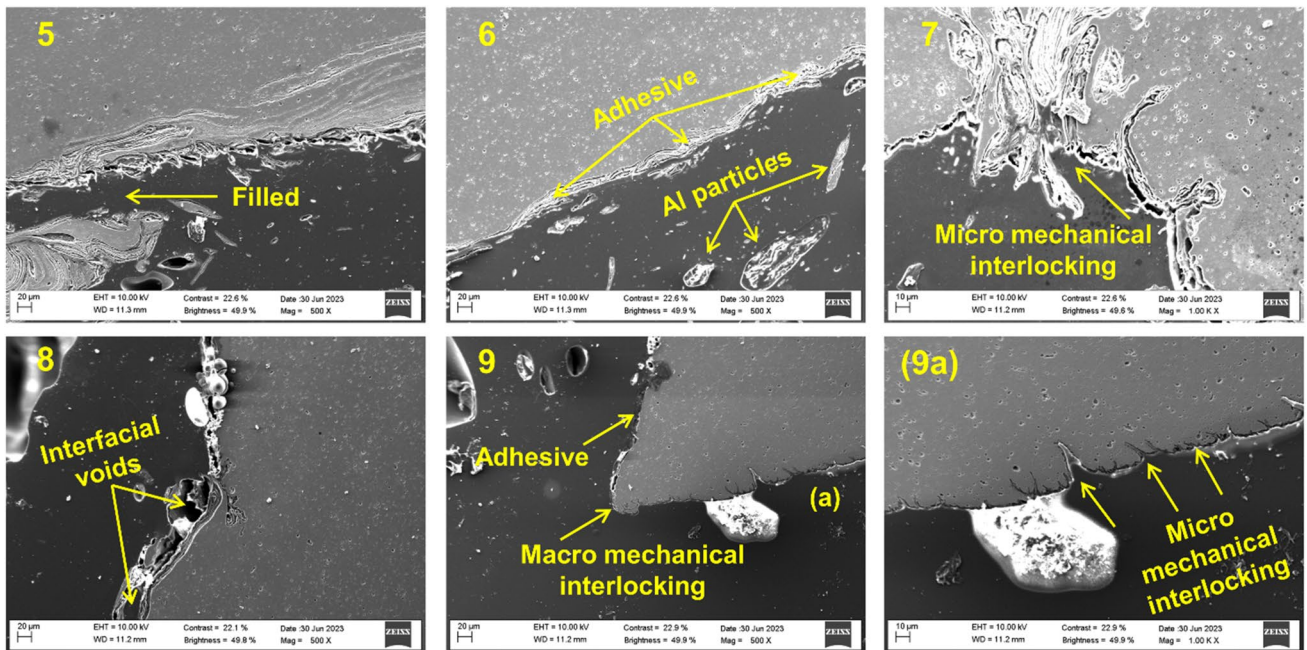
Fig. 17 SEM-based micrographs from points of interest at the interface metal/polymer as identified in Fig. 15 with focus on the centre and flow side (or retreating side)

The centre and flow side of the ceiling of the domain defined by the hook-like feature are assessed via positions 5 and 6, respectively, in Fig. 17. These positions show some bubbles and Al-free particles near the interface but

without interfering with the good wetting with evidence of adhesive effect of the polymer over the metal. The uppermost corner of the interface at the flow side is presented in detail 7 of Fig. 17. This detail presents evidence of several

Fig. 18 SEM-based micrographs from points of interest at the multimaterial interface system AA5754/Ti rigid extrusion die/PEEK, as identified in Fig. 15. This multimaterial interface system is positioned at the shear side of the joint
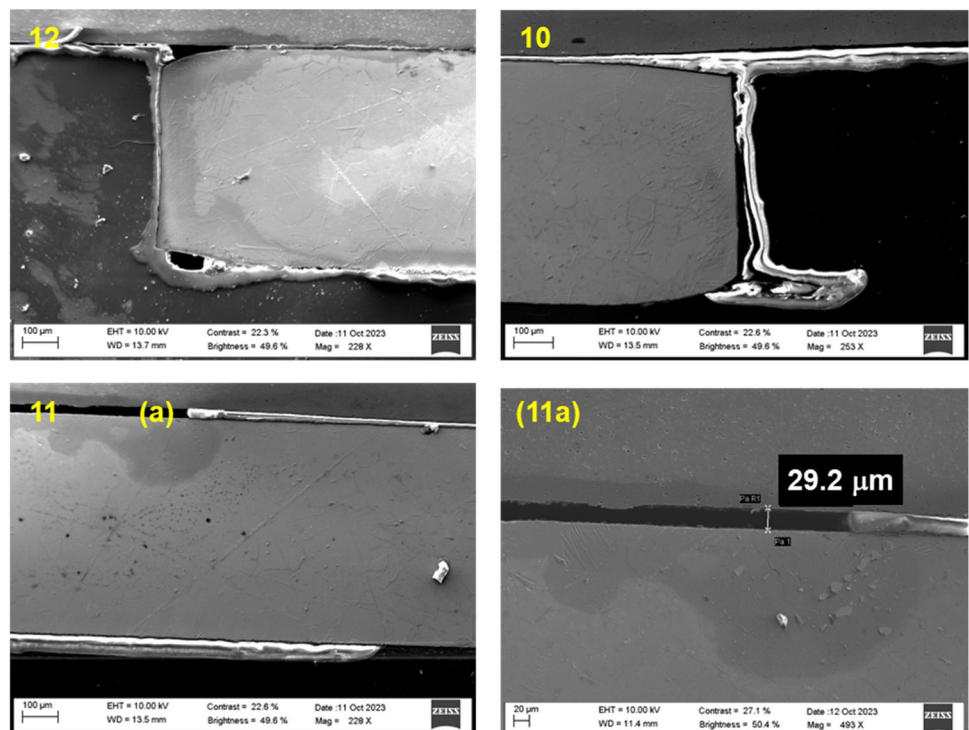
micromechanical anchors supplemented by the formation of some intercalated metal-polymer lamellae structures. Down the flow side along the interface, the adhesive joining is complemented by some interfacial voids as depicted in detail 8 of Fig. 17. Detail 9 of Fig. 17 exhibits the macro-mechanical interlocking provided by the hook-like structural feature at the flow side, assisted by all-around adhesive joining and some micro-mechanical interlocking, including outside the hook-like feature domain, as presented in detail 9a of Fig. 17.

In general, the Fig. 15 presents a better fit (i.e. reduced gap) at the interface between the Ti rigid extrusion die and the PEEK, when compared with the interface between the AA5754 and the Ti rigid extrusion die. Another general aspect depicted by Fig. 15 and emphasized in details 10 and 11 of Fig. 18, is the about 1.5 mm of PEEK of length, which the PEEK flew into the interface AA5754/Ti rigid extrusion die, filling the about 0.3-mm gap between the AA5754 and the Ti rigid extrusion die (detail 11a of Fig. 18). The evidence from the pre-machined slot open in the PEEK surface, to embed the Ti rigid extrusion die (described in Fig. 2a), is still visible at the far side from the centre of the processed zone, i.e. in detail 12 of Fig. 18. Detail 10 of Fig. 18 presents an open lip of PEEK, with about 0.2 mm, aligned with the lower surface of the Ti rigid extrusion die. Under static loading, the fracture modes identified in Fig. 6 do not show any relevant influence from this localized phenomenon. In future research, this aspect should be monitored in terms of acting as site of cracking initiation, under fatigue, or impact loading.

5 Conclusions

The present work demonstrated the influence of probe geometry, and the relative position of the tool axis within the extrusion slot, on the strength and formation of continuous linear TSEJ overlap joints between AA5754 and PEEK. The best overall joint condition is the reference tool probe biased + 1 mm to the flow side within the slot of the extrusion die (trial condition reference: T1 + 1). The best overall joint condition exhibited a maximum average tensile-shear strength of about 110 kN/m, with 1.8 mm deformation at maximum load. From the statistical analysis, there is 84% of the probability of reaching a tensile-shear strength of at least 100 kN/m. For this best overall joint condition, the microstructural analysis emphasizes that all the surface of the hook-like feature is in contact with polymer, including the walls outside the claws.

As joining mechanisms of TSEJ, besides the macro-mechanical interlocking provided by the claws of the double hook-like feature, there is also micro-interlocking created due to the polymer wetting capacity of the roughened profile of the aluminium surface at the joint interface. Some intercalated layers of these materials, and free metallic particles within the polymer, are also depictable at the vicinity of the joining interface. In addition, the voids (closed-porous) in the polymer component, at the vicinity of the interface metal-to-polymer, do not seem to affect the adhesive bonding contribution.

Data availability The management and protection of processed raw data required to reproduce these findings follows best practices in data management policy by Aalto University, and cannot be shared, as these data form part of an ongoing study.

Declarations

Competing interests The authors declare no competing interests.

References

1. Amancio-Filho ST, Dos Santos JF (2009) Joining of polymers and polymer-metal hybrid structures: recent developments and trends. Polym Eng Sci 49:1461–1476. https://doi.org/10.1002/pen.21424

2. Marsh G (2014) Composites and metals – a marriage of convenience? Reinf Plast 58:38–42. https://doi.org/10.1016/S0034-3617(14)70108-0

3. Askeland DR, Wright WJ (2018) Essentials of materials science and engineering. Cengage Learning. https://goo.by/oemflf

4. Cahn RW, Haasen P (Eds.) (1996) Physical metallurgy (Vol. 1). Elsevier. https://goo.by/lZUDEb

5. Maggiore S, Banea MD, Stagnaro P, Luciano G (2021) A review of structural adhesive joints in hybrid joining processes. Polymers 13(22):3961. https://doi.org/10.3390/polym13223961

6. Lambiase F, Scipioni SI, Lee CJ, Ko DC, Liu F (2021) A state-of-the-art review on advanced joining processes for metal-composite and metal-polymer hybrid structures. Materials 14(8):1890. https://doi.org/10.3390/ma14081890

7. Lambiase F, Balle F, Blaga LA, Liu F, Amancio-Filho ST (2021) Friction-based processes for hybrid multi-material joining. Compos Struct 266:113828. https://doi.org/10.1016/j.compstruct.2021.113828

8. Budhe S, Banea MD, De Barros S, Da Silva LFM (2017) An updated review of adhesively bonded joints in composite materials. Int J Adhes Adhes 72:30–42. https://doi.org/10.1016/j.ijadhadh.2016.10.010

9. Huang Y, Meng X, Xie Y, Wan L, Lv Z, Cao J, Feng J (2018) Friction stir welding/processing of polymers and polymer matrix composites. Compos A Appl Sci Manuf 105:235–257. https://doi.org/10.1016/j.composites

10. Messler RW (2004) Joining of materials and structures: from pragmatic process to enabling technology. Butterworth-Heinemann

11. Grote KH, Hefazi H (eds.) (2021) Springer handbook of mechanical engineering (pp 514–543). Springer Nature

12. Katayama S, Kawahito Y (2008) Laser direct joining of metal and plastic. Scripta Mater 59(12):1247–1250. https://doi.org/10.1016/j.scriptamat.2008.08.026

13. Schricker K, Diller S, Bergmann JP (2018) Bubble formation in thermal joining of plastics with metals. Procedia Cirp 74:518–523. https://doi.org/10.1016/j.procir.2018.08.132

14. Falck R, Goushegir SM, dos Santos JF, Amancio-Filho ST (2018) AddJoining: a novel additive manufacturing approach for layered metal-polymer hybrid structures. Mater Lett 217:211–214. https://doi.org/10.1016/j.matlet.2018.01.021

15. Liu FC, Liao J, Nakata K (2014) Joining of metal to plastic using friction lap welding. Mater Des 1980–2015(54):236–244. https://doi.org/10.1016/j.matdes.2013.08.056

16. Liu FC, Nakata K, Liao J, Hirota S, Fukui H (2014) Reducing bubbles in friction lap welded joint of magnesium alloy and polyamide. Sci Technol Weld Joining 19(7):578–587. https://doi.org/10.1179/1362171814Y.0000000228

17. Al-Obaidi A (2018) Ultrasonic joining of metal-polymer surfaces (Doctoral dissertation, University of Sheffield). https://www.researchgate.net/publication/330452244_Ultrasonic_Joining_of_Metal-Polymer_Surfaces

18. Goushegir SM, Dos Santos JF, Amancio-Filho ST (2014) Friction spot joining of aluminum AA2024/carbon-fiber reinforced poly (phenylene sulfide) composite single lap joints: microstructure and mechanical performance. Mater Des 1980–2015(54):196–206. https://doi.org/10.1016/j.matdes.2013.08.034

19. AmancioFilho ST (2011) FRICTION RIVETING: development and analysis of a new joining technique for polymer-metal multi-material structures. Welding in the World 55(1–2):13–24

20. Ratanathavorn W (2012) Hybrid joining of aluminum to thermoplastics with friction stir welding. https://urn.kb.se/resolve?urn=urn:nbn:se:ri:diva-13065

21. Khodabakhshi F, Haghshenas M, Sahraeinejad S, Chen J, Shalchi B, Li J, Gerlich AP (2014) Microstructure-property characterization of a friction-stir welded joint between AA5059 aluminum alloy and high density polyethylene. Mater Charact 98:73–82. https://doi.org/10.1016/j.matchar.2014.10.013

22. Pedro Vilaça, International Application N. WO 2019/002693 A1 (03.01.2019) Method for joining a metal component and a polymer component and a structure comprising said components. Applicant: Aalto University Foundation. WIPO

23. Barakat AA, Darras BM, Nazzal MA, Ahmed AA (2022) A comprehensive technical review of the friction stir welding of metal-to-polymer hybrid structures. Polymers 15(1):220

24. Rudrapati R (2022) Effects of welding process conditions on friction stir welding of polymer composites: a review. Compos C: Open Access 8:100269. https://doi.org/10.1016/j.jcomc.2022.100269

25. Sandeep R, Arivazhagan N (2021) Innovation of thermoplastic polymers and metals hybrid structure using friction stir welding technique: challenges and future perspectives. J Braz Soc Mech Sci Eng 43:1–32. https://doi.org/10.1007/s40430-020-02750-3

26. Li M, Xiong X, Ji S, Hu W, Yue Y (2021) Achieving high-quality metal to polymer-matrix composites joint via top-thermic solid-state lap joining. Compos B Eng 219:108941. https://doi.org/10.1016/j.compositesb.2021.108941

27. Huang Y, Meng X, Wang Y, Xie Y, Zhou L (2018) Joining of aluminum alloy and polymer via friction stir lap welding. J Mater Process Technol 257:148–154. https://doi.org/10.1016/j.jmatprotec.2018.02.043

28. Shahmiri H, Movahedi M, Kokabi AH (2017) Friction stir lap joining of aluminium alloy to polypropylene sheets. Sci Technol Weld Joining 22(2):120–126. https://doi.org/10.1080/13621718.2016.1204171

29. Pedro Vilaça, Prabilson Khadka, Sean Connor Application Nº FI 20227037. Priority date: 15th March 2022. "Method for joining a metal component and a polymer component and a structure comprising said components, – through slot extrusion joining of metal to polymer based component along linear or non-linear path (TSEJ)" Applicant Institution: Aalto University (IPID 3122). Date of filling: 15th March, 2022

30. Pedro Vilaça, Prabilson Khadka, Sean Connor Application Nº FI 20227042. Priority date: 30th March 2022. "Shoulder with inbuilt tapered scrolls" Applicant Institution: Aalto University (IPID 3144). Date of filling: 28th March, 2022

31. Vilaça P, Thomas W (2011) Friction Stir Welding Technology. In: Moreira, P., da Silva, L., de Castro, P. (eds) Structural Connections for Lightweight Metallic Structures. Advanced Structured Materials, vol 8. Springer, Berlin, Heidelberg. https://doi.org/10.1007/8611_2011_56

32. Kaufman JG (2000) Introduction to aluminum alloys and tempers. ASM international

33. Yang S, He Y, Leng J (2020) RecentProgressonPoly (etheretherketone) andItsComposites for Biomedical, Machinery, Energy and Aerospace Applications. Journal of Harbin Institute of Technology (New Series) 27(3). https://doi.org/10.11916/j.issn.1005-9113.2020020

34. Campo EA (2008) 1 - polymeric materials and properties. In: Campo EA (ed) Selection of polymeric materials. William Andrew Publishing, NY, pp 1–39

35. "Alumeco Group," [Online]. Available: https://www.alumeco.fi/alumiini/levyt/valssatut-ja-valetut/en-aw-5754/05-x-1000-x-2000-mm/p/10001398/10003289. [Accessed 15 06 2023]

36. "VINK Finland," [Online]. Available: V. F. Oy., "Vink susta peek natural.https://www.vink.fi/media/import/fi_Vink_SUSTA_PEEK_natural_Datasheet.pdf." .. [Accessed 15 06 2023]

37. "AZO Materials," [Online]. Available: https://www.azom.com/article.aspx?ArticleID=9412. [Accessed 15 06 2023]

38. Iso 14273:2016(en) resistance welding — destructive testing of welds specimen dimensions and procedure for tensile shear testing resistance spot and embossed projection welds. https://www.iso.org/obp/ui/#iso:std:iso:14273:ed-2:v1:en. Accessed 15/06/2023

39. Schricker K, Samfaß L, Grätzel M, Ecke G, Bergmann JP (2020) Bonding mechanisms in laser-assisted joining of metal-polymer composites. J Adv Join Process 1:100008. https://doi.org/10.1016/j.jajp.2020.100008

40. Vasconcelos RL, Oliveira GH, Amancio-Filho ST, Canto LB (2023) Injection overmolding of polymer-metal hybrid structures: a review. Polym Eng Sci 63(3):691–722. https://doi.org/10.1002/pen.26244

41. Courvoisier E, Bicaba Y, Colin X (2016) Water absorption in PEEK and PEI matrices. Contribution to the understanding of water-polar group interactions. In: AIP Conference Proceedings 1736(1). AIP Publishing. https://doi.org/10.1063/1.4949611

42. Vilaça P, Quintino L, dos Santos JF (2005) iSTIR—analytical thermal model for friction stir welding. J Mater Process Technol 169(3):452–465. https://doi.org/10.1016/j.jmatprotec.2004.12.016

43. Vilaça P, Quintino L, dos Santos JF, Zettler R, Sheikhi S (2007) Quality assessment of friction stir welding joints via an analytical thermal model, iSTIR. Mater Sci Eng, A 445:501–508. https://doi.org/10.1016/j.msea.2